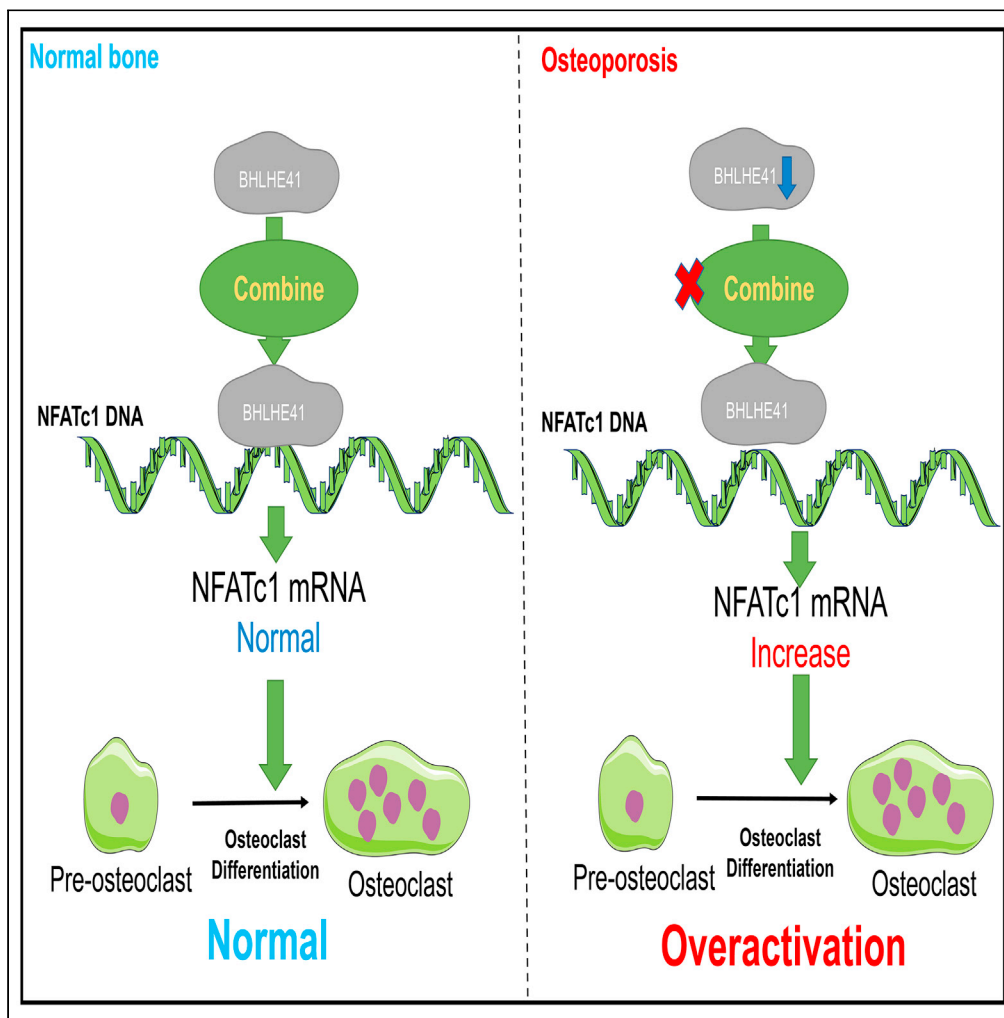**Article**

Basic-helix-loop-helix family member e41 suppresses osteoclastogenesis and abnormal bone resorption disease via NFATc1

Yufeng Zhang, Xiaoguang Li, Jianlong Lang, ..., Wenhui Li, Yi Wang, Liang Zhang

yuf-zhang@tmu.edu.cn (Y.Z.)
wangyi0109@whu.edu.cn (Y.W.)
zhdoctor2008@tmu.edu.cn (L.Z.)

Highlights

BHLHE41 is down-regulated during osteoporosis and osteoclastogenesis

BHLHE41 effectively rescued osteoporosis in mice caused by estrogen deficiency

BHLHE41 suppresses osteoclast differentiation through Nfatc1 signaling

BHLHE41 directly targets Nfatc1

Article

Basic-helix-loop-helix family member e41 suppresses osteoclastogenesis and abnormal bone resorption disease via NFATc1

Yufeng Zhang,[1,3,4,*] Xiaoguang Li,[1,3] Jianlong Lang,[1,3] Wenbo Li,[1] Dengke Huang,[1] Weizong Sun,[1] Li Yang,[1] Wenhui Li,[1] Yi Wang,[2,*] and Liang Zhang[1,*]

SUMMARY

Overactivation of osteoclasts due to altered osteoclastogenesis causes multiple bone metabolic diseases. However, how osteoclast differentiation is tightly regulated and involved in multiple pathophysiological states remains mystery. In this study, we noticed that the downregulation of BHLHE41 (basic-helix-loop-helix family member e41) was tightly associated with osteoclast differentiation and osteoporosis. Functionally, the upregulation or downregulation of BHLHE41 suppressed or promoted osteoclast differentiation, respectively, *in vitro*. A mechanism study indicated that the direct binding of BHLHE41 to the promoter region of NFATc1 that led to its downregulation. Notably, the inhibition of NFATc1 abrogated the enhanced osteoclast differentiation in BHLHE41-knockdown bone marrow macrophages (BMMs). Additionally, upregulation of BHLHE41 impeded bone destruction in OVX mice with osteoporosis. Therefore, our research reveals the mechanism by which BHLHE41 regulates osteoclast differentiation and bone resorption via NFATc1, and targeting BHLHE41 is a potential strategy for the treatment of osteoporosis.

INTRODUCTION

Osteoporosis (OP) is an incurable chronic disease whose incidence increases with ages. OP has become an increasingly troublesome health problem as the world's aging population increases. Osteoporosis affects one in three women and one in five men in the population and is particularly common in postmenopausal women.[1,2] Osteoporosis is a disorder of the bone system characterized by bone loss and microstructural destruction of bone tissue, which increases the risk of loss of bone mass and fragility fractures. In patients with osteoporosis, even minor trauma led to fractures, disability, or death.[3] Bone is a tissue that depends on estrogen, which plays an important role in bone formation and maintenance. During menopause, estrogen deficiency leads to the increased activity of bone resorption and bone formation, yet the bone formation ability is relatively insufficient, which cannot compensate for the bone loss caused by increased bone resorption, which is accompanied by a disorder of the bone trabecular structure, resulting in increased fracture risk.[4,5] Although many antiabsorbent agents are used to inhibit excessive bone resorption in clinical therapy,[6,7] most of them cannot completely prevent bone resorption caused by the overactivation of osteoclasts. Existing drugs have off-target effects and potential side effects,[6,8,9] including mandibular osteonecrosis, cardiovascular events, and gastrointestinal reactions.[10,11] The development of bone therapeutics, such as parathyroid hormone-related peptides and anti-sclerotic monoclonal antibodies, has opened up new avenues for the treatment of osteoporosis.[6] However, their effects last for a very short time, and any discontinuation of treatment leads to rapid bone loss and an increased risk of fractures.[12–14] Hence, it is important to explore a new therapeutic target for osteoporosis.

Osteoclasts (OCs) are the main functional cells responsible for bone resorption and are critical for bone development, growth, repair, and reconstruction. OCs are derived from microenvironmental hematopoietic precursor cells, and OC differentiation is regulated by macrophage colony stimulating factor (M-CSF) and receptor activator of NF-κB ligand (RANKL). RANKL binding to the receptor activator of NF-KB (RANK) activates a variety of signaling pathways, including the MAPK pathway, to stimulate OC differentiation, which leads to bone resorption and destruction.[15] After RANKL binds to RANK, NF-κB, AP-1, NFATC2, ATF4, and JDP2 are recruited to the promoter region of the NFATc1 gene to induce its expression.[16–18] Induced expression of NFATc1 in turn drives the expression of many osteoclast genes, including DC-STAMP, Oscar, OC-STAMP, TRAP, CALCR, CTSK, and other transcription factors (PU.1 and MITF).[19,20] Overactivation of osteoclasts is common in bone diseases, such as malignant bone tumors, osteoporosis, and autoimmune arthritis.[21–23] Therefore, osteoclasts are important targets for the prevention and treatment of bone metabolic diseases in bone.

[1]Department of Orthopedics, The Second Hospital of Tianjin Medical University, Tianjin 300211, China
[2]Department of Pain Management, Zhongnan Hospital of Wuhan University, Wuhan 430071, China
[3]These authors contributed equally
[4]Lead contact
*Correspondence: yuf-zhang@tmu.edu.cn (Y.Z.), wangyi0109@whu.edu.cn (Y.W.), zhdoctor2008@tmu.edu.cn (L.Z.)
https://doi.org/10.1016/j.isci.2024.109059
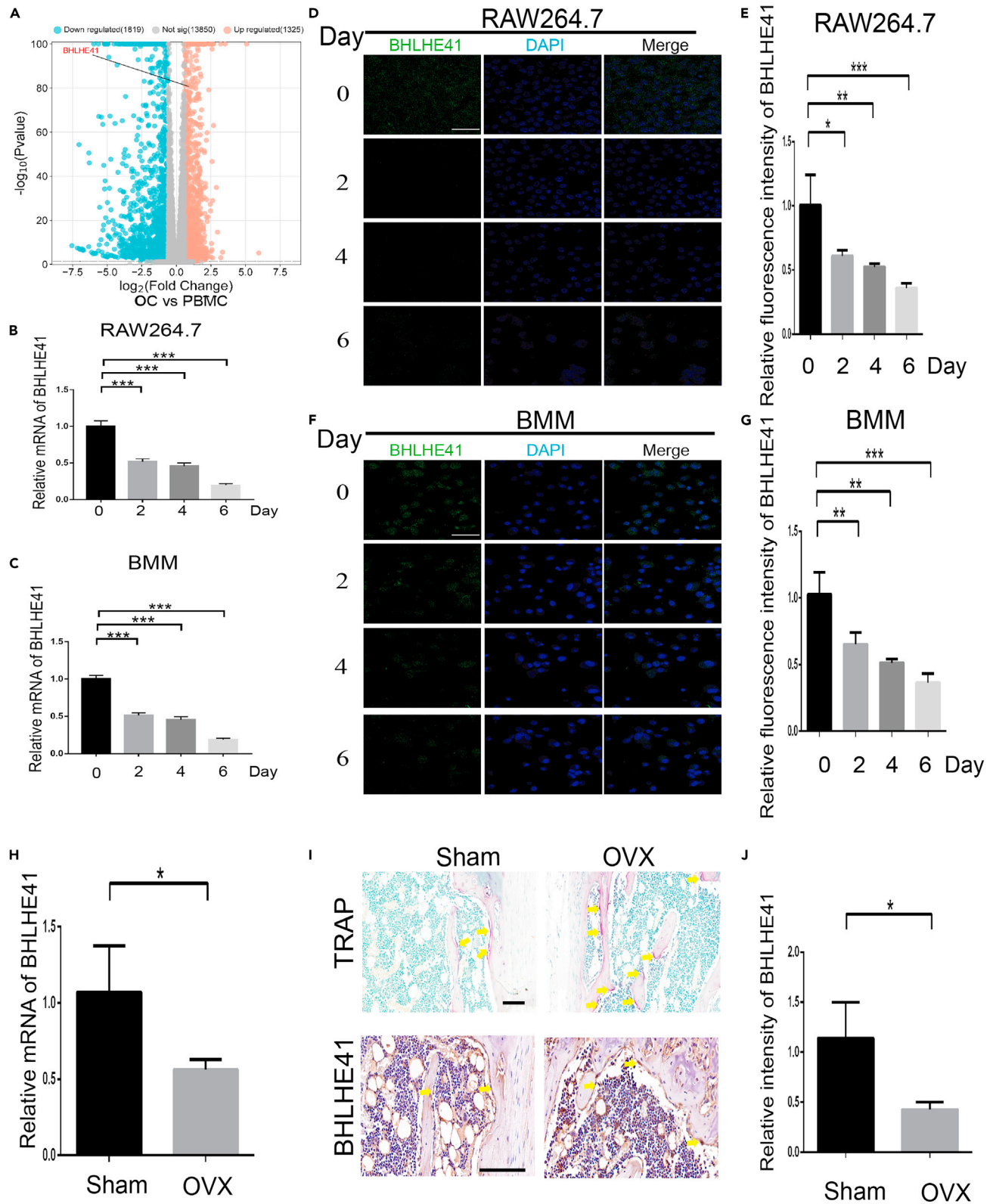
Figure 1. BHLHE41 downregulation was associated with OC differentiation and osteoporosis in mice

(A) Volcano of mRNA in peripheral blood mononuclear cells (PBMCs) and osteoclasts (OCs) from dataset GSE178196 on GEO.

(B) RNA expression of BHLHE41 in RAW264.7 during osteoclast differentiation (n = 3).

(C) RNA expression of BHLHE41 in BMMs during osteoclast differentiation (n = 3).

(D and E) Immunofluorescence and quantitative analysis (n = 3) of BHLHE41 in RAW264.7 during osteoclast differentiation (Scale bar, 50 μm).

(F and G) Immunofluorescence and quantitative analysis (n = 3) of BHLHE41 in BMMs during osteoclast differentiation (Scale bar, 50 μm).

(H) RNA expression of BHLHE41 in BMMs derived from the Sham and OVX groups (n = 3).

(I) TRAP staining and immunohistochemistry of BHLHE41 in femur sections from the OVX and Sham groups (Scale bar, 50 μm).

(J) Quantitative analysis of BHLHE41 expression in immunohistochemistry. All data are means ± SD; *p < 0.05, **p < 0.01, ***p < 0.001.

BHLHE41 (basic-helix-loop-helix family member e41) also known as SHARP1, BHLHB3, and DEC2, is a helix-loop-helix (BHLH) transcription factor that is expressed in a variety of tissues in humans. It plays an important role in regulating cell differentiation, maintaining circadian rhythm, apoptosis, hypoxia, and the immune response.[24–27] BHLHE41 can compete with CLOCK-BMAL1 to regulate circadian rhythm by binding to E-Box elements,[28] and is also associated with multiple signaling pathways, including the Notch, ERK, and PI3K/Akt pathways.[29–31] These functions are crucial for osteoclast formation. Moreover, studies have shown that BHLHE41 inhibits tumor proliferation and metastasis by regulating the ERK/NF-κB pathway in gastric cancer.[29] BHLHE41 also regulates macrophage activity in alveolar cells through cytokines such as IL-5, IL-3, and GM-CSF.[32] In addition, BHLHE41 is an important immunomodulatory agent. Little is known about its role in bone absorption.

In this study, we found that BHLHE41 was downregulated during OC differentiation, and was associated with osteoporosis. We further discovered that BHLHE41 suppresses osteoclastogenesis by inhibiting NFATc1 *in vitro* and *in vivo*. *In vivo*, BHLHE41 overexpression prevented bone impairment in mouse postmenopausal osteoporosis model.

RESULTS

Basic-helix-loop-helix family member e41 downregulation was associated with osteoclasts differentiation and osteoporosis in mice

To investigate the potential role of BHLHE41 in OC differentiation, we analyzed the data of GSE178196 from the Gene Expression Omnibus (GEO) database and found that the Bhlhe41 mRNA was significantly downregulated in RANKL-induced human peripheral blood mononuclear cells (PBMCs) during osteoclastogenesis (Figure 1A). We then induced osteoclast differentiation *in vitro* by M-CSF and RANKL (Figure S1) and found that BHLHE41 mRNA was downregulated in RAW264.7 and BMMs during osteoclast differentiation (Figures 1B and 1C). Downregulation of the BHLHE41 protein in RAW264.7 and BMMs was also observed by immunofluorescence during osteoclastogenesis (Figures 1D–1G). We further established an ovariectomy-induced (OVX) osteoporosis model in mice to verify the correlation of BHLHE41 with postmenopausal osteoporosis and that found BHLHE41 mRNA was downregulated in BMMs derived from ovariectomized mice compared with BMMs derived from control mice (Figure 1H). In addition, immunohistochemistry also showed similar results: the ovariectomized group had more osteoclasts and weaker BHLHE41 expression than did the sham group (Figures 1I and 1J). These results suggest that BHLHE41 may be involved in OC differentiation and bone loss.

Basic-helix-loop-helix family member e41 suppresses osteoclast differentiation *in vitro*

To verify the potential role of BHLHE41 in osteoclastogenesis, we knocked down BHLHE41 with siRNA (Figures 2A and S2A). As evidenced by TRAP staining and phalloidin staining, BMMs with downregulated BHLHE41 had more osteoclasts (Figures 2B–2D). The bone resorption assay showed BMMs with downregulated BHLHE41 had greater ability of bone resorption (Figure 2E). Similarly, compared with si-nc-treated BMMs, si-BHLHE41-treated BMMs exhibited upregulated expression of OC differentiation genes, including the NF-κB receptor activator (RANK), the cellular oncogene fos (c-Fos), the dendritic cell-specific transmembrane protein (DCSTAMP) and the Cathepsin K (CTSK) (Figure 2F). In contrast, overexpression of BHLHE41 (Figures 2G and S2A) induced the opposite phenotype, as shown by TRAP staining, phalloidin staining, and bone resorption assay, which impaired osteoclast differentiation and decreased the expression of OC-specific genes (Figures 2H–2L). In addition, neither upregulation nor downregulation of BHLHE41 expression affected the proliferation of BMM (Figure S2B). These results suggested that BHLHE41 suppressed OC differentiation in mouse BMM.

Basic-helix-loop-helix family member e41 regulates osteoclast differentiation via NFATc1

In order to reveal the potential mechanism by which BHLHE41 suppresses osteoclast differentiation, RNA-seq was performed. A heatmap and volcano analysis identified 970 differentially expressed genes (DEGs) between si-NC and si-BHLHE41 groups, 600 of which were upregulated and 370 of which were downregulated (Figures 3A–3C). KEGG analysis revealed a significant enrichment of genes related to "Cytokine-cytokine receptor interaction", "Rheumatoid arthritis", "PI3K-Akt signaling pathway", "NF-κB signaling pathway" and "MAPK signaling pathway" (Figure 3D), where NF-κB signaling pathway and MAPK signaling pathway was directly related to osteoclast differentiation. Moreover, Gene Ontology (GO) analysis of the DEGs revealed a significant enrichment of genes related to bone remodeling, osteoclast differentiation, ERK1 and ERK2 cascade, and bone resorption (Figures 3E and 3F). The enrichment of genes related to osteoclasts *in vivo* was further analyzed via GOChord. The enriched genes were assigned to the following categories: "osteoclast differentiation", "positive regulation of MAPK cascade", "ERK1 and ERK2 cascade", "bone remodeling", and "regulation of hemopoiesis"
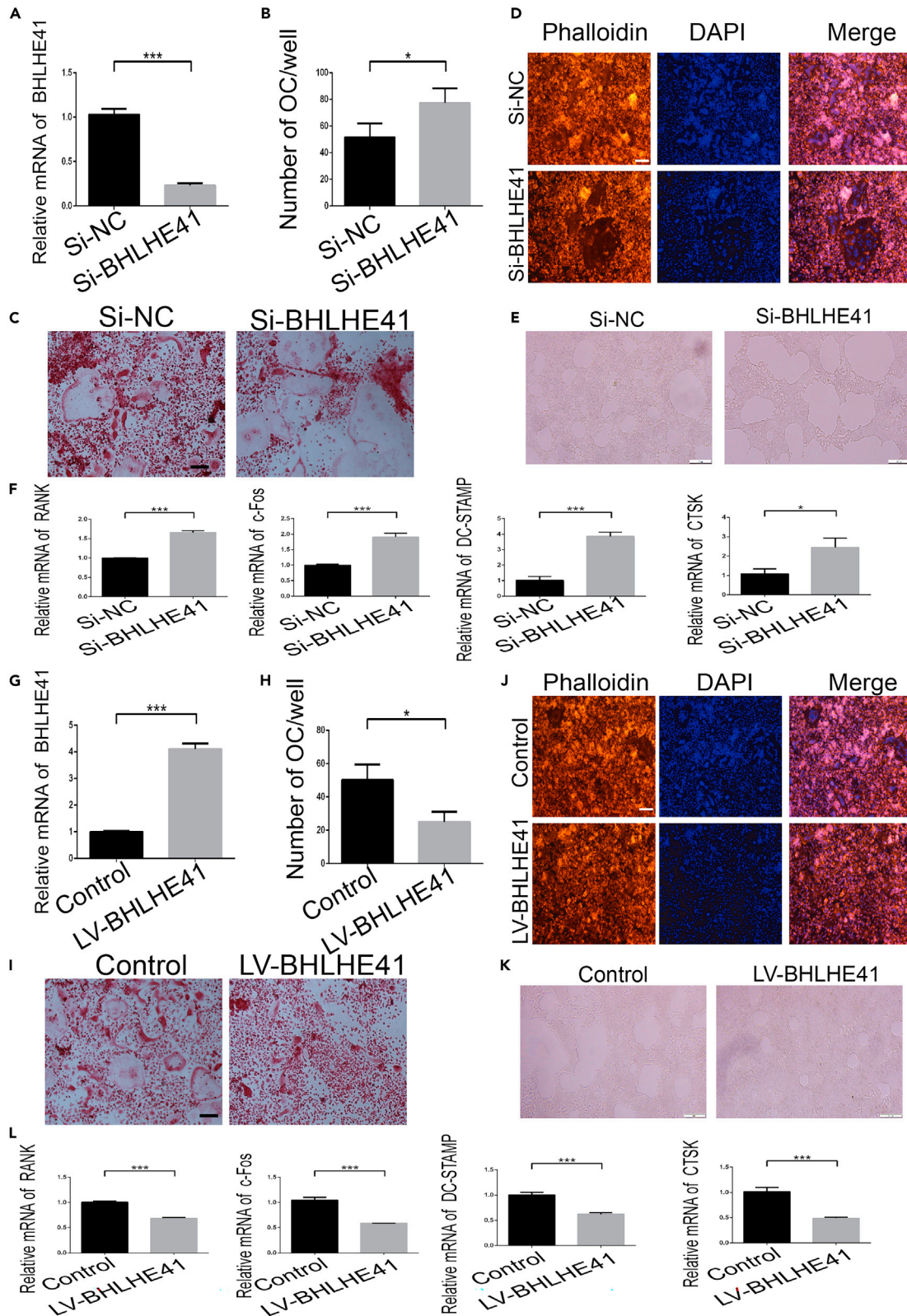
Figure 2. BHLHE41 suppresses osteoclast differentiation in vitro

(A) RNA expression of BHLHE41 in control (si-NC) and BHLHE41 knockdown (si-BHLHE41) of BMMs (n = 3).

(B and C) Quantification (n = 3) and TRAP staining in si-NC and si-BHLHE41 groups (Scale bar, 50 μm).

(D) Phalloidin staining in si-NC and si-BHLHE41 groups (Scale bar, 50 μm).

(E) Bone resorption assay in si-NC and si-BHLHE41 (Scale bar, 100 μm).

(F) RNA expression of OC-specific genes in S si-NC and si-BHLHE41 groups (n = 3).

(G) RNA expression of BHLHE41 in control (Control) and BHLHE41 overexpression (LV-BHLHE41) of BMMs (n = 3).

(H and I) Quantification (n = 3) and TRAP staining in Control and LV-BHLHE41 groups (Scale bar, 50 μm).

(J) Phalloidin staining in Control and LV-BHLHE41 (Scale bar, 50 μm).

(K) Bone resorption assay in Control and LV-BHLHE41 of BMMs (Scale bar, 100 μm).

(L) RNA expression of OC-specific genes in Control and LV-BHLHE41 (n = 3). All data are mean ± SD; *p < 0.05, **p < 0.01, ***p < 0.001.

(Figure 3G). Therefore, we speculated that BHLHE41 might regulate the expression of genes related to osteoclast differentiation. We performed Venn diagram analysis by using BHLHE41 target genes predicted by the Gene Transcriptional Regulation Database (List 1), DEGs between si-NC and si-BHLHE41 groups identified by RNA-seq (List 2), DEGs during osteoclast differentiation which identified by analysis of the GEO database (GSE19950) (List 3), and identified 18 common genes, including NFATc1 (Figure 3H). The changes in the expression of 18 genes in the si-NC and si-BHLHE41 groups were verified by qRT-PCR (MEF2C, CHAF1A, WWP1, BRCA1, MATK, CREBRF, C1QBP, CSTB, CCNF, ASNS, AK2, STX11, MAN2A2, DUSP4, NFATC1, BCAR3, PGM2L1, and ATP6V1D) (Figure S3A). However, only 5 genes were further confirmed in Bhlhe41 overexpressing cells, and no significant changes in DUSP4, AK2, WWP1, and STX11 expression were observed (Figure S3B). Taken together, these results suggested that BHLHE41 may suppress osteoclastogenesis by regulating the master regulator NFATc1.

### Basic-helix-loop-helix family member e41 directly targeted NFATc1

To further investigate the regulatory role of BHLHE41 in NFATc1 expression, we analyzed the correlation between BHLHE41 and NFATc1 (GSE56815) in the GEO database, and found that the p value between BHLHE41 and NFATc1 was 0.0078 (Figure 4A). Indeed, we further verified that the downregulation of BHLHE41 induced an increase in the protein expression of NFATc1 (Figures 4B and 4C), while the upregulation of BHLHE41 decreased the expression of NFATc1 in BMMs (Figures 4D and 4E). These observations suggested that BHLHE41 regulated NFATc1 during osteoclast differentiation. To explore whether BHLHE41 directly regulated NFATc1, 2 putative BHLHE41-binding sites were identified in the NFATc1 gene promoter region by JASPAR (http://jaspar.genereg.net) (Figure 4F). ChIP analysis of the BHLHE41 antibody-treated cells revealed that the amount of DNA in the putative binding site (−1715bp ∼ −1706bp) was significantly greater than that in the preimmune control antibody (Figure 4G). To test whether NFATc1 is involved in Bhlhe41-mediated osteoclastogenesis, NFATc1 was knocked down by siRNA (Figure S2C) in BHLHE41 downregulation cells. NFATc1 knockdown abrogated the enhanced osteoclastogenesis induced by BHLHE41 downregulation, as evidenced by a decrease in TRAP+ cells and osteoclast-specific gene expression (Figures 4H–4J). Consistent with these findings, treatment with a NFATc1 inhibitor (NFAT inhibitor) also produced similar results (Figures 4K–4M). These findings demonstrated that BHLHE41 directly bound to the promoter regions of the NFATc1 genes and regulated its expression.

Activation of basic-helix-loop-helix family member e41 alleviates bone loss due to estrogen deficiency and osteoporosis

To investigate whether BHLHE41 could be a potential therapeutic target for bone loss in osteoporosis, we generated an ovariectoid osteoporosis mouse model, and then BHLHE41-overexpressing or control lentivirus was administered via bone marrow injection (Figure 5A). Micro-CT revealed that OVX mice that were administered the BHLHE41-overexpressing lentivirus had higher bone mass, Tb. N and Tb.Th, and lower Tb. Pf than OVX mice that were administered the control lentivirus, while there was no significant change in trabecular separation (Figures 5B and 5C). These results suggested that activating BHLHE41 can effectively prevent bone loss in estrogen-deficient osteoporosis. Similarly, H&E staining showed that OVX did not significantly change bone mass or Tb. N in BHLHE41-overexpressing mice but did so in control mice (Figures 5D and 5E). There were more TRAP-positive cells in the OVX mice which were administered control lentivirus mice than in the Sham mice whereas no significant changes were observed between the OVX mice which were administered the BHLHE41-overexpressing lentivirus and the Sham mice (Figures 5F and 5G). Moreover, the increase in BHLHE41 and the inhibition of NFATc1 in the BHLHE41-overexpressing group were confirmed by immunohistochemical analysis (Figures 5H and 5I). These findings suggested that BHLHE41 may play an important role in osteoporosis, especially OVX-induced osteoporosis.

DISCUSSION

Transcriptional regulation is the basic mechanism of gene expression, which can regulate many biological processes including the cell cycle, differentiation, and apoptosis.[33,34] During transcription, RNA polymerase temporarily stops transcription under the control of certain factors and continues to extend transcription when conditions are met. Osteoclasts, the main bone resorption cells in the bone marrow,[35] are controlled by the combined action of multiple transcription factors, some of which may have a wider range of expression. BHLHE41 is a helix-loop-helix transcription factor that plays a key role in a variety of biological processes and is expressed in a variety of human tissues and cells,[36,37] including macrophages.[32] Although Hirata found that the mRNA expression of BHLHE41 was downregulated during osteoclast
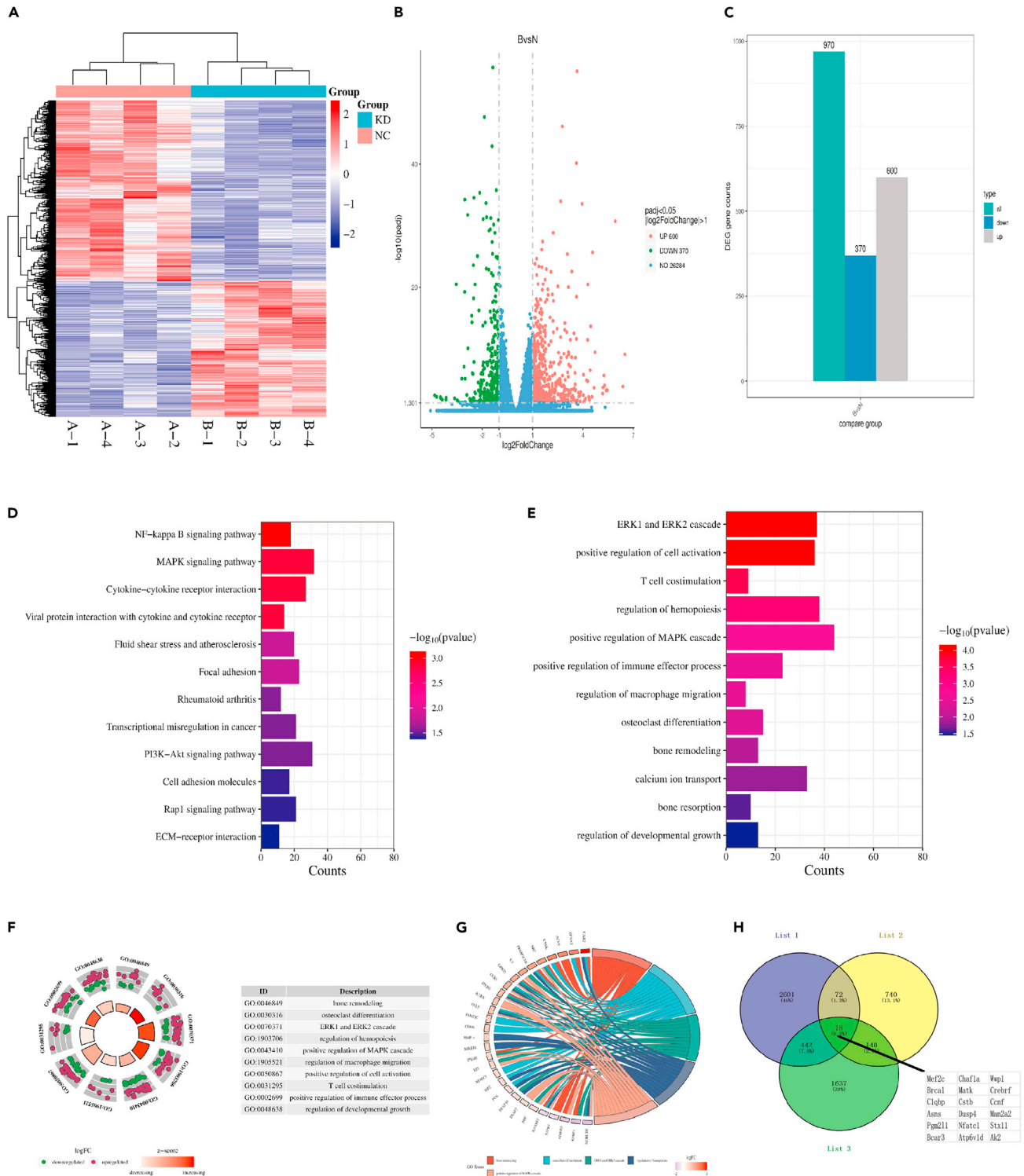
Figure 3. BHLHE41 regulates osteoclast differentiation via NFATc1

(A) Heatmap of differentially expressed genes (DEGs) for BMMs in si-NC and si-BHLHE41 groups (n = 4).

(B and C)Volcano plot and quantification of RNA-seq data of BMMs in si-NC and si-BHLHE41 groups.

(D) GOBubble plot of KEGG enrichment analysis in DEGs.

(E) GOBubble plot of GO enrichment analysis in DEGs.

(F) GOCircle plot of GO enrichment analysis of the DEGs.

Figure 3. *Continued*

(G) GOchord of GO enrichment analysis of DEGs, including "ERK1 and ERK2 cascade", "bone remodeling", "regulation of hemopoiesi", "positive regulation of MAPK cascade", and "osteoclast differentiation."

(H) The predicted result of downstream genes regulated by BHLHE41. List1 mentioned BHLHE41 binding genes. List2 mentioned the significantly changed genes between si-NC and si-BHLHE41 which identified by RNA-seq. List3 mentioned significant changes in genes during osteoclast differentiation which identified by analysis of the GEO database (GSE19950).

differentiation, this study focused mainly on Bhlhe40-mediated bone resorption through regulating the production of acid in osteoclasts and did not further investigate the role and mechanism of BHLHE41 in osteoclast differentiation.[38] However, the role of BHLHE41 in osteoclastogenesis remains unclear.

Here, we demonstrated that the downregulation of BHLHE41 was associated with abnormal bone resorption diseases, and BHLHE41 was downregulated in the early stage of osteoclastogenesis, which is considered the key stage of osteoclast differentiation.[39] Moreover, knockdown or overexpression of BHLHE41 promoted or inhibited osteoclast differentiation, respectively. Through RNA-seq and chromatin immunoprecipitation, we identified a new BHLHE41/NFATc1 axis through which BHLHE41 effects osteoclastogenesis. In addition, we treated osteoporotic mice with upregulated BHLHE41 and found significant improvement in abnormal bone resorption, indicating that BHLHE41 is an effective way to treat postmenopausal osteoporosis.

Our RNA-seq and subsequent experiments indicated that BHLHE41 affects osteoclastogenesis by regulating the transcription of NFATc1. NFATc1 promotes the expression of various osteoclast differentiation-specific genes and is regulated by a variety of transcription factors and signaling molecules.[40–42] Indeed, downregulation or inhibition of NFATc1 significantly reversed the increase in osteoclast differentiation in BHLHE41 knockdown BMMs, suggesting that the regulation of osteoclast formation by BHLHE41 is dependent on NFATc1. Our ChIP-PCR confirmed that BHLHE41 directly binds to the promoter region of the NFATc1 gene. Moreover, transcriptome analysis revealed that the downregulation of BHLHE41 induced multiple signaling pathways, including the MAPK, NF-κB, and ERK pathways. These signaling pathways play a very important role in osteoclast differentiation,[43] among which the NF-κB signaling pathway is correlated with the expression of NFATc1.[40]

Osteoporosis is a common bone remodeling disease associated with a variety of factors, such as age, menopause, and chronic diseases, including type I and type II osteoporosis. Type I osteoporosis, also known as postmenopausal osteoporosis, is caused by postmenopausal estrogen deficiency and affects mainly trabecular bone absorption. Postmenopausal osteoporosis usually occurs in women between the ages of 50 and 65, which also marks the end of a woman's conception phase. Type II osteoporosis, also known as senile osteoporosis, is characterized by age-related loss of cortical and trabecular in humans. For osteolytic diseases caused by excessive osteoclasts, bone resorption inhibitors such as bisphosphonates and selective estrogen receptor modulators (SERMs) are used clinically to regulate osteoclast function and inhibit excessive bone resorption [48]. However, bone resorption inhibitors do not treat existing osteoporosis. Most drugs have off-target effects and potential side effects [13, 69], and some drugs even cause withdrawal and severe side effects after long-term treatment [7, 9–12]. For refractory abnormal bone resorption diseases such as hereditary osteosclerosis and malignant osteoporosis, bone marrow transplantation is even required [70, 71], and these treatments cause great pain to patients. Here, we investigated animal models of OVX-induced bone destruction and found BHLHE41 may be a potential target for the treatment of osteoclast overactivation. Upregulation BHLHE41 can inhibit osteoclastogenesis and prevent excessive bone resorption. Trabecular number, trabecular thickness, and trabecular separation were used to evaluate the cancellous bone structure. The bone mass and trabecular number of ovariectomized mice with upregulated BHLHE41 expression were greater than those in the control group and similar to those in the sham operation group. In addition, pathological analysis revealed that ovariectomized mice with upregulated BHLHE41 expression had significantly fewer osteoclasts than control mice did, which demonstrated BHLHE41 could prevent bone loss by inhibiting osteoclastogenesis. Considering the side effects of the treatment of osteoporosis, BHLHE41 could be a potential target for treating osteoporosis in the future.

Limitations of the study

This study reveals the mechanism by which BHLHE41 regulates osteoclast differentiation and bone resorption via NFATc1, and targeting BHLHE41 is a potential strategy for the treatment of osteoporosis. Although we discussed the inhibitory effect of BHLHE41 on osteoclastic differentiation, the effect of BHLHE41 deficiency on bone development was not revealed *in vivo*, and BHLHE41-specific knockout mice are considered necessary in future studies. In addition, our previous study found that BHLHE40 can also regulate osteoclastogenic differentiation by regulating the transcription of NFATc1. However, whether there is an interaction between BHLHE41 and BHLHE40 to regulate the transcription of NFATc1 remains to be further investigated.

STAR★METHODS

Detailed methods are provided in the online version of this paper and include the following:

- KEY RESOURCES TABLE
- RESOURCE AVAILABILITY
  - Lead contact
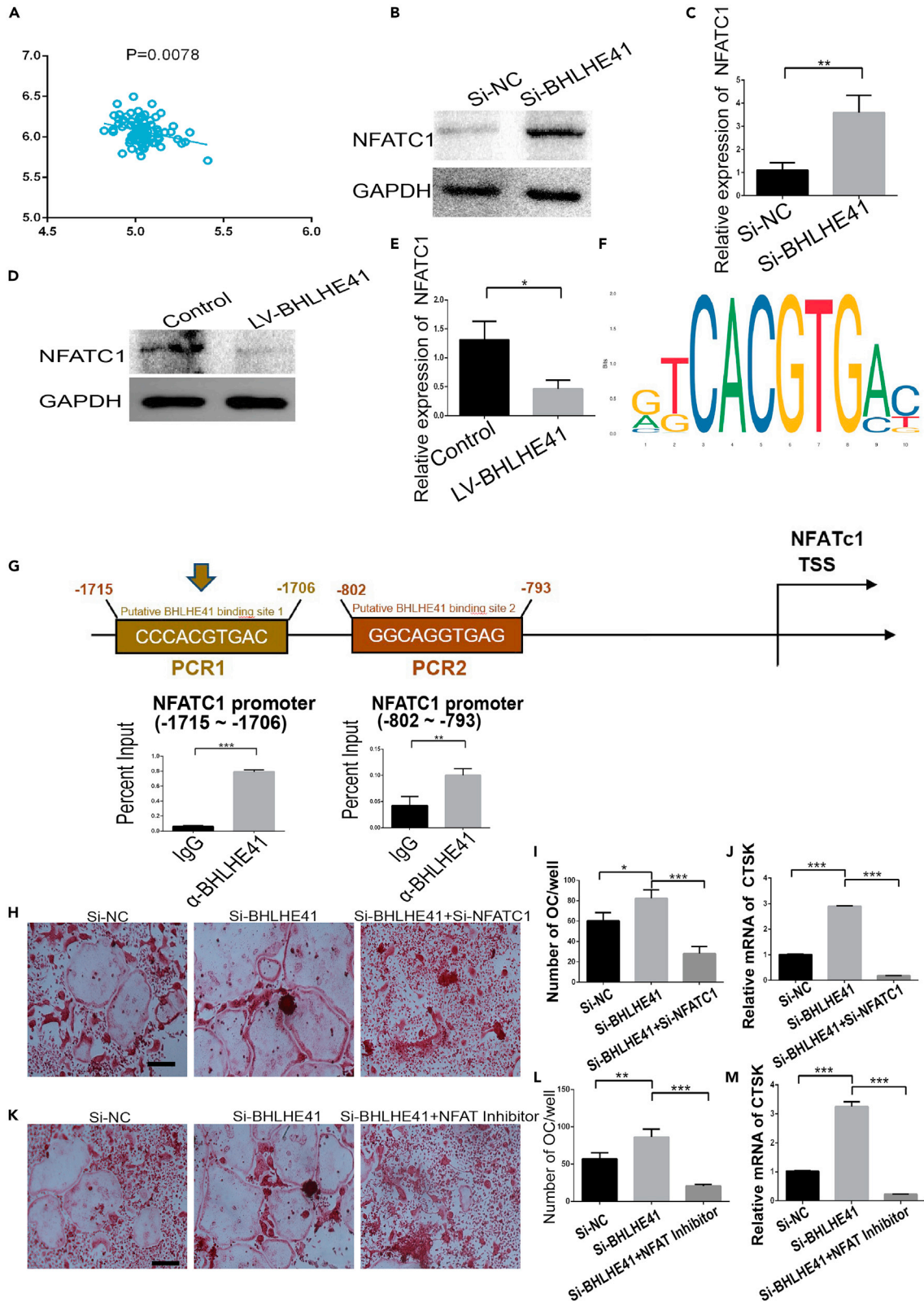
Figure 4. BHLHE41 directly targeted NFATc1

(A) The correlation expression of BHLHE41 and NFATc1 (GSE56815 dataset) (n = 80).

(B and C) Western blotting and quantification (n = 3) to detect the expression of NFATc1 in si-NC and si-BHLHE41 in BMMs.

(D and E) Western blotting and quantification (n = 3) to detect the expression of NFATc1 in Control and LV-BHLHE41 in BMMs.

(F) Motif of BHLHE41 promoter binding site.

(G) Anti-BHLHE41 ChIP assay for the NFATc1 promoter in BMMs. Predicted Anti-BHLHE41 binding sites are indicated. Immunoprecipitated DNA was amplified by qPCR (n = 3). Normal rabbit IgG was used as a negative control. Results are presented as ChIP/Input.

(H and I) TRAP staining and quantification (n = 3) to detect the osteoclast differentiation of BMMs in Control, BHLHE41 Overexpression and BHLHE41 Overexpression treated with si-NFATc1 (Scale bar, 50 μm).

(J) OC-specific genes expression of BMMs in Control, BHLHE41 Overexpression and BHLHE41 Overexpression treated with si-NFATc1 (n = 3).

(K and L) TRAP staining and quantification (n = 3) to detect the osteoclast differentiation of BMMs in Control, BHLHE41 Overexpression and BHLHE41 Overexpression treated with NFAT Inhibitor (Scale bar, 50 μm).

(M) OC-specific genes expression of BMMs in Control, BHLHE41 Overexpression and BHLHE41 Overexpression treated with NFAT Inhibitor (n = 3). NFAT Inhibitor reduced the expression of NFATc1. All data are mean $\pm$ SD; *p < 0.05, **p < 0.01, ***p < 0.001.

- ○ Materials availability
- ○ Data and code availability
- ● EXPERIMENTAL MODEL AND STUDY PARTICIPANT DETAILS
    - ○ Cell lines
    - ○ Animals
- ● METHOD DETAILS
    - ○ Osteoclast differentiation
    - ○ Animal experiments
    - ○ Knockdown and overexpression
    - ○ Chromatin immunoprecipitation (ChIP)
    - ○ RNA extraction and quantitative PCR
    - ○ Western blotting
    - ○ Micro-CT analysis
    - ○ Immunohistochemistry and histological analysis
    - ○ Immunofluorescence staining
    - ○ Transcriptomic analysis
    - ○ Bioinformatics analysis
- ● QUANTIFICATION AND STATISTICAL ANALYSIS

SUPPLEMENTAL INFORMATION

Supplemental information can be found online at https://doi.org/10.1016/j.isci.2024.109059.

AUTHOR CONTRIBUTIONS

Conceptualization, Y.F.Z., X.G.L., and L.Z.; methodology, Y.F.Z. and X.G.L.; software, Y.F.Z.; validation, Y.F.Z., X.G.L., and J.L.L.; formal analysis, Y.F.Z. and W.B.L.; investigation, Y.F.Z., J.L.L., and D.K.H.; resources, W.Z.S. and L.Z.; data curation, Y.F.Z., L.Y., and W.H.L.; writing—original draft preparation, Y.F.Z.; writing—review and editing, Y.F.Z., X.G.L., and L.Z.; visualization, Y.F.Z. and Y.W.; supervision, L.Z.; project administration, L.Z.; funding acquisition, L.Z. The authors Y.F.Z., X.G.L., and J.L.L. contributed equally. All authors have read and agreed to the published version of the article.
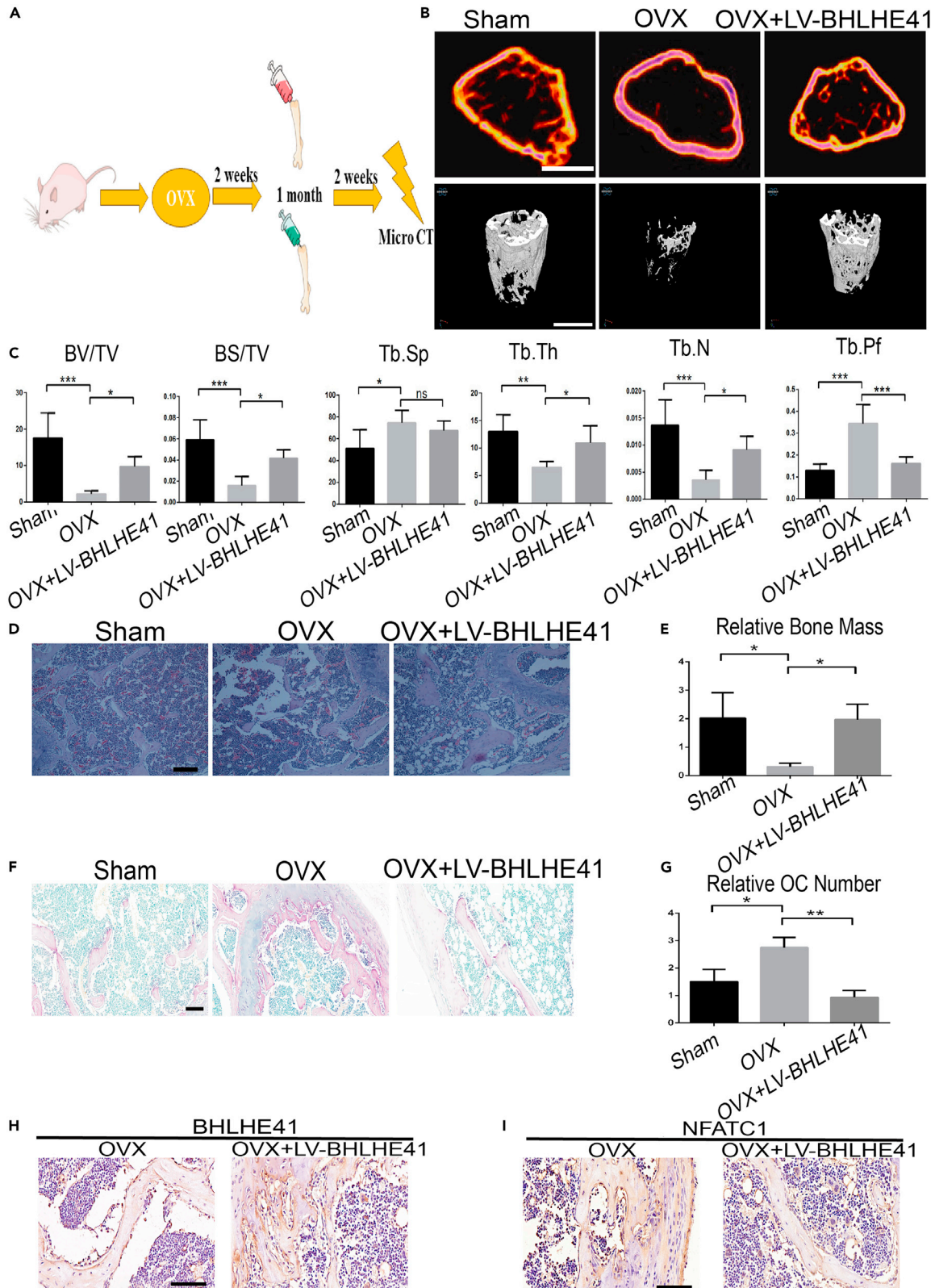
DECLARATION OF INTERESTS

The authors declare no competing interests.

Figure 5. Activation of BHLHE41 alleviates bone loss due to estrogen deficiency osteoporosis

(A) Schematic diagram of the treatment of OVX mice.

(B) Representative μCT images (Scale bars, 0.5 mm).

(C) Quantification of femur parameters by μCT from sham, therapy and control mice. Tb. Sp; Tb. Pf; Tb. N; Tb. Th; BV/TV; BS/TV (n = 5).

(D and E) H&E staining and quantification (n = 5) of femur sections from Sham, OVX and OVX mice treated with BHLHE41 overexpressed lentivirus therapy (Scale bar, 100 μm).

(F and G) TRAP staining and quantification (n = 5) of femur sections from Sham, OVX and OVX with BHLHE41 overexpressed lentivirus therapy (Scale bar, 50 μm).

(H) Immunohistochemistry of BHLHE41 in femur sections from OVX mice treated with Control and BHLHE41 overexpressed lentivirus (Scale bar, 50 μm).

(I) Immunohistochemistry of NFATc1 in femur sections from OVX mice treated with Control and BHLHE41 overexpressed lentivirus (Scale bar, 50 μm). All data are means ± SD; *p < 0.05, **p < 0.01, ***p < 0.001.

REFERENCES

1. Wang, Q.S., Wang, G.F., Lu, Y.R., Cui, Y.L., Li, H., Li, R.X., Zhang, X.Z., Zhang, C.Q., and Liu, T.J. (2018). The Combination of icariin and constrained dynamic loading stimulation attenuates bone loss in ovariectomy-induced osteoporotic mice. J. Orthop. Res. 36, 1415–1424. https://doi.org/10.1002/jor.23777.

2. Yu, F., and Xia, W. (2019). The epidemiology of osteoporosis, associated fragility fractures, and management gap in China. Arch. Osteoporosis 14, 32. https://doi.org/10.1007/s11657-018-0549-y.

3. Compston, J.E., McClung, M.R., and Leslie, W.D. (2019). Osteoporosis. Lancet (London, England) 393, 364–376. https://doi.org/10.1016/s0140-6736(18)32112-3.

4. Noh, J.Y., Yang, Y., and Jung, H. (2020). Molecular Mechanisms and Emerging Therapeutics for Osteoporosis. Int. J. Mol. Sci. 21, 7623. https://doi.org/10.3390/ijms21207623.

5. Li, H., Xiao, Z., Quarles, L.D., and Li, W. (2021). Osteoporosis: Mechanism, Molecular Target and Current Status on Drug Development. Curr. Med. Chem. 28, 1489–1507. https://doi.org/10.2174/0929867327666200330142432.

6. Seeman, E., and Martin, T.J. (2019). Antiresorptive and anabolic agents in the prevention and reversal of bone fragility. Nat. Rev. Rheumatol. 15, 225–236. https://doi.org/10.1038/s41584-019-0172-3.

7. Bone, H.G., Wagman, R.B., Brandi, M.L., Brown, J.P., Chapurlat, R., Cummings, S.R., Czerwiński, E., Fahrleitner-Pammer, A., Kendler, D.L., Lippuner, K., et al. (2017). 10 years of denosumab treatment in postmenopausal women with osteoporosis: results from the phase 3 randomised FREEDOM trial and open-label extension. Lancet Diabetes Endocrinol. 5, 513–523. https://doi.org/10.1016/s2213-8587(17)30138-9.

8. Drake, M.T., Clarke, B.L., Oursler, M.J., and Khosla, S. (2017). Cathepsin K Inhibitors for Osteoporosis: Biology, Potential Clinical Utility, and Lessons Learned. Endocr. Rev. 38, 325–350. https://doi.org/10.1210/er.2015-1114.

9. Gartrell, B.A., Coleman, R.E., Fizazi, K., Miller, K., Saad, F., Sternberg, C.N., and Galsky, M.D. (2014). Toxicities following treatment with bisphosphonates and receptor activator of nuclear factor-κB ligand inhibitors in patients with advanced prostate cancer. Eur. Urol. 65, 278–286. https://doi.org/10.1016/j.eururo.2013.05.015.

10. Fink, H.A., MacDonald, R., Forte, M.L., Rosebush, C.E., Ensrud, K.E., Schousboe, J.T., Nelson, V.A., Ullman, K., Butler, M., Olson, C.M., et al. (2019). Long-Term Drug Therapy and Drug Discontinuations and Holidays for Osteoporosis Fracture Prevention: A Systematic Review. Ann. Intern. Med. 171, 37–50. https://doi.org/10.7326/m19-0533.

11. Kendler, D.L., Marin, F., Zerbini, C.A.F., Russo, L.A., Greenspan, S.L., Zikan, V., Bagur, A., Malouf-Sierra, J., Lakatos, P., Fahrleitner-Pammer, A., et al. (2018). Effects of teriparatide and risedronate on new fractures in post-menopausal women with severe osteoporosis (VERO): a multicentre, double-blind, double-dummy, randomised controlled trial. Lancet (London, England) 391, 230–240. https://doi.org/10.1016/s0140-6736(17)32137-2.

12. Leder, B.Z., Tsai, J.N., Uihlein, A.V., Wallace, P.M., Lee, H., Neer, R.M., and Burnett-Bowie, S.A.M. (2015). Denosumab and teriparatide transitions in postmenopausal osteoporosis (the DATA-Switch study): extension of a randomised controlled trial. Lancet (London, England) 386, 1147–1155. https://doi.org/10.1016/s0140-6736(15)61120-5.

13. Balani, D.H., Ono, N., and Kronenberg, H.M. (2017). Parathyroid hormone regulates fates of murine osteoblast precursors in vivo. J. Clin. Invest. 127, 3327–3338. https://doi.org/10.1172/jci91699.

14. Honvo, G., Bannuru, R.R., Bruyère, O., Rannou, F., Herrero-Beaumont, G., Uebelhart, D., Cooper, C., Arden, N., Conaghan, P.G., Reginster, J.Y., et al. (2019). Recommendations for the Reporting of Harms in Manuscripts on Clinical Trials Assessing Osteoarthritis Drugs: A Consensus Statement from the European Society for Clinical and Economic Aspects of Osteoporosis, Osteoarthritis and Musculoskeletal Diseases (ESCEO). Drugs & aging 36, 145–159. https://doi.org/10.1007/s40266-019-00667-8.

15. Kim, J.H., and Kim, N. (2016). Signaling Pathways in Osteoclast Differentiation. Chonnam Med. J. 52, 12–17. https://doi.org/10.4068/cmj.2016.52.1.12.

16. Ohori, F., Kitaura, H., Marahleh, A., Kishikawa, A., Ogawa, S., Qi, J., Shen, W.R., Noguchi, T., Nara, Y., and Mizoguchi, I. (2019). Effect of TNF-α-Induced Sclerostin on Osteocytes during Orthodontic Tooth Movement. J. Immunol. Res. 2019, 9716758. https://doi.org/10.1155/2019/9716758.

17. Yang, X., Han, X., Shu, R., Jiang, F., Xu, L., Xue, C., Chen, T., and Bai, D. (2016). Effect of sclerostin removal in vivo on experimental periodontitis in mice. J. Oral Sci. 58, 271–276. https://doi.org/10.2334/josnusd.15-0690.

18. Kullander, K., and Klein, R. (2002). Mechanisms and functions of Eph and ephrin signalling. Nat. Rev. Mol. Cell Biol. 3, 475–486. https://doi.org/10.1038/nrm856.

19. Wang, R., Luo, H., Yang, D., Yu, B., Guo, J., Shao, L., Okamura, H., and Qiu, L. (2023). Osteoblast Jmjd3 regulates osteoclastogenesis via EphB4 and RANKL signalling. Oral Dis. 29, 1613–1621. https://doi.org/10.1111/odi.14160.

20. Menale, C., Campodoni, E., Palagano, E., Mantero, S., Erreni, M., Inforzato, A., Fontana, E., Schena, F., Van't Hof, R., Sandri, M., et al. (2019). Mesenchymal Stromal Cell-Seeded Biomimetic Scaffolds as a Factory of Soluble RANKL in Rankl-Deficient Osteopetrosis. Stem Cells Transl. Med. 8, 22–34. https://doi.org/10.1002/sctm.18-0085.

21. Shapouri-Moghaddam, A., Mohammadian, S., Vazini, H., Taghadosi, M., Esmaeili, S.A., Mardani, F., Seifi, B., Mohammadi, A., Afshari, J.T., and Sahebkar, A. (2018). Macrophage plasticity, polarization, and function in health and disease. J. Cell. Physiol. 233, 6425–6440. https://doi.org/10.1002/jcp.26429.

22. Orecchioni, M., Ghosheh, Y., Pramod, A.B., and Ley, K. (2019). Macrophage Polarization: Different Gene Signatures in M1(LPS+) vs. Classically and M2(LPS-) vs. Alternatively Activated Macrophages. Front. Immunol. 10, 1084. https://doi.org/10.3389/fimmu.2019.01084.

23. De Santa, F., Vitiello, L., Torcinaro, A., and Ferraro, E. (2019). The Role of Metabolic Remodeling in Macrophage Polarization and Its Effect on Skeletal Muscle Regeneration. Antioxidants Redox Signal. 30, 1553–1598. https://doi.org/10.1089/ars.2017.7420.

24. Sato, F., Otsuka, T., Kohsaka, A., Le, H.T., Bhawal, U.K., and Muragaki, Y. (2019). Smad3 Suppresses Epithelial Cell Migration and Proliferation via the Clock Gene Dec1, Which Negatively Regulates the Expression of Clock Genes Dec2 and Per1. Am. J. Pathol. 189, 773–783. https://doi.org/10.1016/j.ajpath.2019.01.006.

25. Sato, H., Wu, Y., Kato, Y., Liu, Q., Hirai, H., Yoshizawa, T., Morohashi, S., Watanabe, J., and Kijima, H. (2017). DEC2 expression antagonizes cisplatin-induced apoptosis in human esophageal squamous cell carcinoma. Mol. Med. Rep. 16, 43–48. https://doi.org/10.3892/mmr.2017.6571.

26. Kreslavsky, T., Vilagos, B., Tagoh, H., Poliakova, D.K., Schwickert, T.A., Wöhner, M., Jaritz, M., Weiss, S., Taneja, R., Rossner, M.J., and Busslinger, M. (2017). Essential role for the transcription factor Bhlhe41 in regulating the development, self-renewal and BCR repertoire of B-1a cells. Nat. Immunol. 18, 442–455. https://doi.org/10.1038/ni.3694.

27. Grampp, S., Schmid, V., Salama, R., Lauer, V., Kranz, F., Platt, J.L., Smythies, J., Choudhry, H., Goppelt-Struebe, M., Ratcliffe, P.J., et al. (2017). Multiple renal cancer susceptibility polymorphisms modulate the HIF pathway. PLoS Genet. 13, e1006872. https://doi.org/10.1371/journal.pgen.1006872.

28. Hirano, A., Hsu, P.K., Zhang, L., Xing, L., McMahon, T., Yamazaki, M., Ptáček, L.J., and Fu, Y.H. (2018). DEC2 modulates orexin

expression and regulates sleep. Proc. Natl. Acad. Sci. USA *115*, 3434–3439. https://doi.org/10.1073/pnas.1801693115.

29. Li, P., Jia, Y.F., Ma, X.L., Zheng, Y., Kong, Y., Zhang, Y., Zong, S., Chen, Z.T., and Wang, Y.S. (2016). DEC2 suppresses tumor proliferation and metastasis by regulating ERK/NF-κB pathway in gastric cancer. Am. J. Cancer Res. *6*, 1741–1757.

30. Oswald, F., Kostezka, U., Astrahantseff, K., Bourteele, S., Dillinger, K., Zechner, U., Ludwig, L., Wilda, M., Hameister, H., Knöchel, W., et al. (2002). SHARP is a novel component of the Notch/RBP-Jkappa signalling pathway. The EMBO journal *21*, 5417–5426. https://doi.org/10.1093/emboj/cdf549.

31. Wu, Y., Sato, H., Suzuki, T., Yoshizawa, T., Morohashi, S., Seino, H., Kawamoto, T., Fujimoto, K., Kato, Y., and Kijima, H. (2015). Involvement of c-Myc in the proliferation of MCF-7 human breast cancer cells induced by bHLH transcription factor DEC2. Int. J. Mol. Med. *35*, 815–820. https://doi.org/10.3892/ijmm.2014.2042.

32. Rauschmeier, R., Gustafsson, C., Reinhardt, A., A-Gonzalez, N., Tortola, L., Cansever, D., Subramanian, S., Taneja, R., Rossner, M.J., Sieweke, M.H., et al. (2019). Bhlhe40 and Bhlhe41 transcription factors regulate alveolar macrophage self-renewal and identity. The EMBO journal *38*, e101233. https://doi.org/10.15252/embj.2018101233.

33. Chan, W.C.W., Tan, Z., To, M.K.T., and Chan, D. (2021). Regulation and Role of Transcription Factors in Osteogenesis. Int. J. Mol. Sci. *22*, 5445. https://doi.org/10.3390/ijms22115445.

34. Karimian, A., Ahmadi, Y., and Yousefi, B. (2016). Multiple functions of p21 in cell cycle, apoptosis and transcriptional regulation after DNA damage. DNA Repair *42*, 63–71. https://doi.org/10.1016/j.dnarep.2016.04.008.

35. Ono, T., and Nakashima, T. (2018). Recent advances in osteoclast biology. Histochem. Cell Biol. *149*, 325–341. https://doi.org/10.1007/s00418-018-1636-2.

36. Zhang, D., Zheng, Q., Wang, C., Zhao, N., Liu, Y., and Wang, E. (2020). BHLHE41 suppresses MCF-7 cell invasion via MAPK/JNK pathway. J. Cell Mol. Med. *24*, 4001–4010. https://doi.org/10.1111/jcmm.15033.

37. Wang, X., Sato, F., Tanimoto, K., Rajeshwaran, N., Thangavelu, L., Makishima, M., and Bhawal, U.K. (2021). The Potential Roles of Dec1 and Dec2 in Periodontal Inflammation. Int. J. Mol. Sci. *22*, 10349. https://doi.org/10.3390/ijms221910349.

38. Hirata, H., Kamohara, A., Murayama, M., Nishioka, K., Honda, H., Urano, Y., Soejima, H., Oki, S., Kukita, T., Kawano, S., et al. (2022). A novel role of helix-loop-helix transcriptional factor Bhlhe40 in osteoclast activation. J. Cell. Physiol. *237*, 3912–3926. https://doi.org/10.1002/jcp.30844.

39. Park, J.H., Lee, N.K., and Lee, S.Y. (2017). Current Understanding of RANK Signaling in Osteoclast Differentiation and Maturation. Mol. Cell. *40*, 706–713. https://doi.org/10.14348/molcells.2017.0225.

40. Asagiri, M., and Takayanagi, H. (2007). The molecular understanding of osteoclast differentiation. Bone *40*, 251–264. https://doi.org/10.1016/j.bone.2006.09.023.

41. Negishi-Koga, T., and Takayanagi, H. (2009). Ca2+-NFATc1 signaling is an essential axis of osteoclast differentiation. Immunol. Rev. *231*, 241–256. https://doi.org/10.1111/j.1600-065X.2009.00821.x.

42. Kim, I., Kim, J.H., Kim, K., Seong, S., and Kim, N. (2019). The IRF2BP2-KLF2 axis regulates osteoclast and osteoblast differentiation. BMB Rep. *52*, 469–474. https://doi.org/10.5483/BMBRep.2019.52.7.104.

43. Ding, D., Yan, J., Feng, G., Zhou, Y., Ma, L., and Jin, Q. (2022). Dihydroartemisinin attenuates osteoclast formation and bone resorption via inhibiting the NF-κB, MAPK and NFATc1 signaling pathways and alleviates osteoarthritis. Int. J. Mol. Med. *49*, 4. https://doi.org/10.3892/ijmm.2021.5059.

44. Zhang, Y., Yang, M., Zhang, S., Yang, Z., Zhu, Y., Wang, Y., Chen, Z., Lv, X., Huang, Z., Xie, Y., and Cai, L. (2022). BHLHE40 promotes osteoclastogenesis and abnormal bone resorption via c-Fos/NFATc1. Cell Biosci. *12*, 70. https://doi.org/10.1186/s13578-022-00813-7.

45. Ma, Z., Li, L., Livingston, M.J., Zhang, D., Mi, Q., Zhang, M., Ding, H.F., Huo, Y., Mei, C., and Dong, Z. (2020). p53/microRNA-214/ULK1 axis impairs renal tubular autophagy in diabetic kidney disease. J. Clin. Invest. *130*, 5011–5026. https://doi.org/10.1172/jci135536.

46. Bouxsein, M.L., Boyd, S.K., Christiansen, B.A., Guldberg, R.E., Jepsen, K.J., and Müller, R. (2010). Guidelines for assessment of bone microstructure in rodents using micro-computed tomography. J. Bone Miner. Res. *25*, 1468–1486. https://doi.org/10.1002/jbmr.141.

47. Gautier, E.L., Shay, T., Miller, J., Greter, M., Jakubzick, C., Ivanov, S., Helft, J., Chow, A., Elpek, K.G., Gordonov, S., et al. (2012). Gene-expression profiles and transcriptional regulatory pathways that underlie the identity and diversity of mouse tissue macrophages. Nat. Immunol. *13*, 1118–1128. https://doi.org/10.1038/ni.2419.

48. Mass, E., Ballesteros, I., Farlik, M., Halbritter, F., Günther, P., Crozet, L., Jacome-Galarza, C.E., Händler, K., Klughammer, J., Kobayashi, Y., et al. (2016). Specification of tissue-resident macrophages during organogenesis. Science *353*. https://doi.org/10.1126/science.aaf4238.

49. Okabe, Y., and Medzhitov, R. (2016). Tissue biology perspective on macrophages. Nat. Immunol. *17*, 9–17. https://doi.org/10.1038/ni.3320.

50. Michalski, M.N., and McCauley, L.K. (2017). Macrophages and skeletal health. Pharmacol. Ther. *174*, 43–54. https://doi.org/10.1016/j.pharmthera.2017.02.017.

STAR★METHODS

KEY RESOURCES TABLE

REAGENT or RESOURCE	SOURCE	IDENTIFIER
Antibodies		
BHLHB3 Antibody	Affnity	Cat#AF0442; RRID: AB_2834318
Anti-rabbit IgG, HRP-linked Antibody	CST	Cat# 7074; RRID: AB_2099233
NFATc1 Antibody	Affnity	Cat#DF6446; RRID: AB_2838409
GAPDH Antibody	Proteintech Group In	Cat# 60004-1-Ig; RRID: AB_2107436
Secondary antibody	Abcam	Cat#ab150077; RRID: AB_2630356
Bacterial and virus strains		
Si-NC	RiboBio	N/A
Si-BHLHE41(5′ to 3′): CCCGAACATCTGAAATTGA	RiboBio	N/A
Si-NFATc1(5′ to 3′): CCCGTCCAAGTCAGT TTCTAT	RiboBio	N/A
BHLHE41 overexpression plasmid	Shanghai Genechem	N/A
Chemicals, peptides, and recombinant proteins		
rmM-CSF	R&D Systems	Cat#416-ML-010
rmRANKL	R&D Systems	Cat#462-TEC-010
4% paraformaldehyde	Beyotime	Cat# P0099-500ml
Triton-X	Beyotime	Cat#ST795
Tartrate-resistant acid phosphatase (TRAP) solution	Servicebio	Cat#G1050
Phalloidin	Servicebio	Cat#G1041
DAPI	Servicebio	Cat#G1012
NFAT Inhibitor	MCE	Cat#HY-P1026
Immunoprecipitation lysate	Servicebio	Cat#G2038
Protease inhibitor cocktail	MCE	Cat#HY-K0010
RNase A	Sigma-Aldrich	Cat#R6513
proteinase K	MCE	Cat#HY-108717
TRIzol	Thermo Fisher	Cat#15596026
Phosphatase inhibitor cocktail I	MCE	Cat#HY-K0021
Polink-2 Plus polymer HRP detection system	ZSBG-BIO	Cat#PV6001
DAB	ZSBG-BIO	Cat#ZLI-9017
Critical commercial assays		
cDNA using reverse transcriptase kit	Vazyme	Cat#R223
SYBR green mixture	Vazyme	Cat#Q311
Total RNA Extraction Kit	Epoch Life Sciences	Cat#1660050
riboFECT CP Transfection Kit	RiboBio	Cat#R10035.7
TIANGEN Common DNA Product Purification Kit	TIANGEN	Cat#DP204
Deposited data		
Transcriptome arrays of osteoclastogenesis	This paper	GEO: GSE178196
The correlation of BHLHE41 and NFATc1	This paper	GEO: GSE56815
Experimental models: Cell lines		
Human embryonic kidney 293 T cells	ATCC	Cat#CRL-3216™
RAW264.7	ATCC	Cat#TIB-71™

Continued

REAGENT or RESOURCE	SOURCE	IDENTIFIER
Mouse BMMs	Isolated from bone marrow	N/A
Experimental models: Organisms/strains		
C57BL/6J	Si Beifu Biotechnology Co., LTD (Beijing, China)	N/A
Oligonucleotides		
Primers in this paper, see STAR Methods for Knockdown and overexpression, Chromatin immunoprecipitation and RNA extraction and quantitative PCR	This paper	N/A
Software and algorithms		
Prism	GraphPad	N/A
Adobe Illustrator	N/A	N/A
SkyScan 1276 high-resolution micro-CT imaging system	Bruker	N/A
NRecon	Bruker	N/A
CTAn	Bruker	N/A
LAS X	Leica	N/A
Tanon-5200	Tanon	N/A
Image-Pro Plus 6.0	N/A	N/A
Monad Real-Time PCR instrument	Monad	N/A
Inverted microscope system	Olympus	IX73
Other		
Bone resorption assay plate	Cosmo Bio	Cat#CSR-BRA-48P
Ultracel-100 regenerated cellulose membrane, 15 mL sample volume	Millipore	Cat# UFC9100
A/G magnetic beads	MCE	Cat#HY-K0202
α-MEM	HyClone	Cat# SH30265.01B

RESOURCE AVAILABILITY

Lead contact

Further information and requests for resources and reagents should be directed to and will be fulfilled by the lead contact, Dr. Yufeng Zhang (yuf-zhang@tmu.edu.cn).

Materials availability

This study did not generate new unique reagents.

Data and code availability

- All data reported in this paper will be shared by the lead contact upon request.
- This paper does not report original code.
- Any additional information required to reanalyze the data reported in this paper is available from the lead contact upon request.

EXPERIMENTAL MODEL AND STUDY PARTICIPANT DETAILS

Cell lines

The mouse macrophage cell line RAW264.7 (ATCC, Cat#TIB-71™) and the human kidney epithelial cell line 293T (ATCC, Cat#CRL-3216™) were cultured in DMEM containing 10% fetal bovine serum (FBS) at 37°C in an atmosphere of 5% CO_2.

Bone marrow macrophages (BMMs) were isolated from 4-week-old male C57BL/6J mice. In brief, the femurs were separated under sterile conditions and the marrow cavity was rinsed with α-MEM (HyClone, Cat# SH30265.01B) containing 10% fetal bovine serum and 1%

penicillin-streptomycin. Cell suspensions were cultured overnight in complete α-MEM at 37°C and 5% CO_2. The supernatant was transferred to a new cell culture flask, M-CSF was added to a final concentration of 50 ng/ml, and the cells were cultured for another 3 days.

Animals

All animal experimental procedures were in accordance with protocols approved by Institutional Animal Care and Use Committee of Wuhan University (WP20230615). Since this study focused on postmenopausal osteoporosis models, female mice were used as experimental animals. Four-week-old female C57BL/6J mice purchased from Si Beifu Biotechnology Co., LTD (Beijing, China).

METHOD DETAILS

Osteoclast differentiation

For OC differentiation, cells were cultured in complete α-MEM containing 50 ng/ml M-CSF (R&D Systems, Cat#416-ML-010) and 50 ng/ml RANKL (R&D Systems, Cat#462-TEC-010) for 6 days.[44] The medium was replaced every other day. Mature osteoclasts were fixed in 4% paraformaldehyde at room temperature for 20 minutes, soaked in PBS containing 0.5% Triton-X for 30 minutes, and stained with tartrate-resistant acid phosphatase (TRAP) solution (Servicebio, Cat#G1050) at 37°C for 30 minutes. DAPI (Servicebio, Cat#G1012) and phalloidin (Servicebio, Cat#G1041) were used for cytoskeleton staining. Fluorescence images were obtained using an inverted microscope system (Olympus, IX73). Cells with three or more nuclei were counted. Statistics are based on the number of OCs in 8 fields. For the bone resorption assay, BMMs were inoculated on a bone resorption assay plate (Cosmo Bio, Cat#CSR-BRA-48P), M-CSF was added to a final concentration of 50 ng/ml, and the cells were cultured for another 1 day. Then, cells were cultured in complete α-MEM containing 50 ng/ml M-CSF and 50 ng/ml RANKL for 6 days. The cells were cleared by soaking in 5% sodium hypochlorite for 3 minutes. Images were obtained using an inverted microscope system (Olympus, IX73). NFATc1 was inhibited with 10μM NFAT Inhibitor (MCE, Cat#HY-P1026).

Animal experiments

To establish an osteoporosis mouse model,[44] 8-week-old C57BL/6 female mice were anesthetized with 1-4% isoflurane, and a 0.5 cm unilateral midline dorsal incision was made through the skin on the lower back. The connective tissue under the skin was removed, and a small incision was made on each side to reach the abdominal cavity. The fallopian tubes and ovaries were exposed, the ovaries were located, and the fallopian tubes were ligated. Sterile scissors were used to gently cut the fallopian tubes, and the ovaries were removed. The remaining fallopian tubes were returned to the abdominal cavity, and the tubes were closed layer by layer. For the lentivirus injection experiment, For the lentivirus injection experiment, 20 μl of BHLHE41-overexpressing or control lentivirus was injected into the femoral bone marrow cavity ($2.5*10^{10}$μg/ml) every 7 days for 4 weeks at the 3rd week after surgery.

Knockdown and overexpression

To knock down BHLHE41 and NFATc1, 24 hours after cell adhesion, riboFECT CP Transfection Kit (RiboBio, Cat #R10035.7) was used for 100nM siRNA transfection for 24 hours. The BHLHE41 overexpression plasmid was purchased from Shanghai Genechem, and lentivirus packaging and infection were performed as previously described. In brief, the pSPAX2, pMD2. G and the target plasmids were cotransfected into 293T cells to package the lentivirus. The supernatant was collected at 48 hours and 72 hours to concentrate the lentivirus. (Millipore, Ultracel-100 regenerated cellulose membrane, 15 mL sample volume, Cat# UFC9100). Lentiviral infection (MOI=100) of BMMs was performed in the presence of 10 μg/ml polybrene for 24 hours. Cells were selected with 2 μg/ml puromycin for 72 hours. The knockdown efficiency or overexpression level of BHLHE41 or NFATc1 was verified by qPCR.

The target siRNA gene sequences were as follows: BHLHE41 siRNA: 5′-CCCGAACATCTGAAATTGA-3′ and NFATc1 siRNA: 5′-CCCGTCCAAGTCAGTTTCTAT-3′.

Chromatin immunoprecipitation (ChIP)

BMMs were cultured in 50 ng/ml M-CSF for 3 days and fixed in 1% formaldehyde at room temperature for 10 minutes.[45] The cells were neutralized with glycine and cell lysate was collected. The cells were resuspended in 4°C ultrasound buffer for 10 minutes, and then each sample was ultrasonicated 6 times with 40% AMP for 15 seconds. Chromatin was collected from the supernatant after centrifugation at 4°C at 8000 g for 30 seconds, and 50μl samples were taken to extract input DNA. The input DNA was purified using TIANGEN Common DNA Product Purification Kit (TIANGEN, Cat#DP204), after incubating with 1μl of 1mg/ml RNase A (Sigma-Aldrich, Cat# R6513) and 2μl of proteinase K (20 mg/ml) at 65°C overnight. The chromatin samples were incubated with 40 μl prebalanced protein A/G magnetic beads (MCE, Cat#HY-K0202) for 2 hours at 4°C. After the beads were removed, 1μg of anti-BHLHE41 antibody was added and incubated overnight, after which the proteins were precipitated with protein A/G magnetic beads. The beads were washed and DNA was eluted and purified with TIANGEN Common DNA Product Purification Kit after RNase A treatment. Immunoprecipitated DNA fragments were collected for qPCR amplification. Normal rabbit IgG was used as negative control. DNA samples were analyzed by real-time quantitative PCR and IgG was standardized.

The primer sequences were as follows:
NFATc1(-1715∼-1706): Forward(F): 5′-CTCAGGAGCCAAGGGCAG-3′/Reverse(R): 5′-CTCCTTCTCCCCACCTCCAG-3′
NFATc1(-802∼-793): Forward(F): 5′-GAGGAAAGTGTGAGTGGCCG-3′/Reverse(R): 5′-CCGGGACGTCGAGTTATTGT-3′
The primary antibodies included: BHLHE41 (Affinity, Cat#AF0442, 1:100) or Anti-rabbit IgG, HRP-linked Antibody (CST, Cat# 7074, 1:100).

RNA extraction and quantitative PCR

Total RNA was extracted from cells by TRIzol (Thermo Fisher, Cat#15596026).[45] 200 ng total RNA was reverse transcribed into cDNA using reverse transcriptase kit (Vazyme, Cat#R223). SYBR green mixture (Vazyme, Cat#Q311) and Monad Real-Time PCR instrument (Monad q225) was used for quantitative PCR.

The primer sequences were as follows:
NFATc1: Forward(F):5′-TATATGAGCCCATCCTTGCCT-3′/Reverse(R):5′-GGCTGCCTTCCGTCTCATAG-3′
RANK: F:5′-CTCCTTGGAAAGCTAGAAGCAC-3′/R:5′-TTCCCTCCCTTCCTGTAGTAAAC-3′
CTSK: F:5′-GCACCCTTAGTCTTCCGCTC-3′/R:5′-GGTCATATAGCCGCCTCCAC-3′
BHLHE41: F: 5′-GGAGCTTGAAGCGAGACGAT-3′/R: 5′- GAGCGCTCCCCATTCTGTAA-3′
DCSTAMP: F: 5′-TCCTCCATGAACAAACAGTTCCA-3′/R: 5′-AGACGTGGTTTAGGAATGCAGCTC-3′
c-Fos: F: 5′-TGTTCCTGGCAATAGCGTGT-3′/R: 5′-TCAGACCACCTCGACAATGC-3′
GAPDH: F:5′-TGAAGGGTGGAGCCAAAAG-3′/R:5′-AGTCTTCTGGGTGGCAGTGAT-3′
CHAF1A: F:5′-GGATTGCAAAGACAGACCCG-3′/R:5′-ACTGGCTTGATTGTTGCCCT-3′
MATK: F:5′-TAGTGAGACCGGCGCTAGG-3′/R:5′-AGGCAGGTCCCTAGATTCCC-3′
CSTB: F: 5′-CCTCCCCCATGAAAACAAGC-3′/R: 5′- AGAAGCTGCTCAACTCCCTTC-3′
MEF2C: F: 5′-TTGACGATCAAGGGGGCAAA-3′/R: 5′-TGCCTTTCTGCTTCTCCAGG-3′
BRCA1: F: 5′-GAGGATCCAGCACCTCTCTTG-3′/R: 5′-CAAAGGACATTGTGAAGGCCC-3′
C1QBP: F:5′-CTCTGCACACGGAAGGAGAC-3′/R:5′-CCGTGATCTTTTCTCCGGCA-3′
ATP6V1D: F:5′-TTGCCTCTTAGCAACGCAGT-3′/R:5′-GTCTTTGCCCGACATCCTGA-3′
AK2: F:5′-CCTGATCCGCAGGTCAGATG-3′/R:5′-ACCACCCACTCCTTTCACAG-3′
BCAR3: F: 5′-TGCCTGGCCTCTGAATTAGG-3′/R: 5′- GACTTTTCCCCTCCGCTGAA-3′
ASNS: F: 5′-TTTGCCTGGGACTAGGTGGA-3′/R: 5′-AACAGATTTTTCCCGGCGTG-3′
PGM2L1: F: 5′-GTTGTTGTTCTCTCGCCTCAC-3′/R: 5′-TCAGCCATGGTAGACACACG-3′
DUSP4: F:5′-GGCACTTGGCTAAACTGGTC-3′/R:5′-TGCCAGTTGTCTGGTACAGC-3′
MAN2A2: F:5′-GCCGCGTACGCTCCG-3′/R:5′-AAGATAGCAGCCCCACACAC-3′
STX11: F: 5′-CCCGCAGGATCACGGTTC-3′/R: 5′- AGACCGGTTCTACGCTCTCT-3′
WWP1: F: 5′-GTAAATGTGACCCCACAGACCA-3′/R: 5′-CGGTTTGTTACAGGCTCTTGC-3′
CCNF: F: 5′-CCACCGCAGAGCTATCGAAT-3′/R: 5′-GACATCACCCTCCTTCTCGC-3′
CREBRF: F:5′-CTTCAGCCTCAGAACCGCAAA-3′/R:5′-GGTCCATTCCGCTTACGCT-3′

Western blotting

Proteins were extracted from the cells by immunoprecipitation lysate (Servicebio, Cat#G2038) containing protease inhibitor cocktail (MCE, Cat#HY-K0010, 1:100) and phosphatase inhibitor cocktail I (MCE, Cat#HY-K0021, 1:100). After standing on ice for 30 minutes, the extract was centrifuged at 13000 rpm for 15 minutes, to collect protein. For Western blotting analysis, 25ug denatured total protein was separated with via 10% SDS-PAGE gel. Tanon-5200 (Tanon, 18000856) and Image-Pro Plus 6.0 were used for the detection and analysis of immunoreactive proteins. The protein level was normalized to the level of GAPDH.

The primary antibodies included: BHLHE41 (Affinity, Cat#AF0442, 1:1000) , NFATc1 (Affinity, Cat#DF6446, 1:1000) or GAPDH (Proteintech Group In, Cat# 60004-1-Ig, 1:4000). GAPDH was used as a control.

Micro-CT analysis

All mice were euthanized with CO_2, the femurs were separated and evaluated with the SkyScan 1276 high-resolution micro-CT imaging system (Bruker). According to the manufacturer's instructions,[46] each femur was scanned by a 0.25 mm aluminum filter at 55 kV and 200 μA to obtain an isometric resolution of 8-μm. NRecon (Bruker) was used to reconstruct the images and CTAn (Bruker) was used for quantitative analysis. The trabecular bone parameters in an area from 0.2 mm to 2.3 mm below the growth plate of the femur were measured, including bone surface to total volume ratio (BS/TV), bone volume to total volume ratio (BV/TV), trabecular bone number (Tb. N), trabecular bone thickness (Tb. Th), trabecular separation (Tb. Sp), trabecular pattern factor (Tb. Pf).

Immunohistochemistry and histological analysis

For paraffin sections, the femurs were fixed with 4% paraformaldehyde for 48 hours, decalcified with 10% EDTA for 28 days, and then embedded in paraffin. The slices were sliced with Leica RM2235 microtome (8 μm), dewaxed and stained with TRAP (Servicebio, Cat. # G1050) and hematoxylin-eosin (H&E).

For immunohistochemistry, sections were dewaxed and treated with citrate buffer at 95°C (pH 6.0) 3 times and 3% H2O2 at room temperature for 20 minutes. The samples were then blocked with 5% bovine serum albumin (BSA) at room temperature for 1 hour and incubated with primary antibody at 4°C overnight. After the samples were washed, Polink-2 Plus polymer HRP detection system (ZSBG-BIO, Cat#PV6001) was used for secondary antibody incubation of samples, DAB (ZSBG-BIO, Cat#ZLI-9017) was used for color rendering. Hematoxylin was used for nuclear staining.

The primary antibodies included: BHLHE41 (Affinity, Cat#AF0442, 1:200) or NFATc1 (Affinity, Cat#DF6446, 1:200).

Immunofluorescence staining

BMMs and RAW264.7 were cultured in complete α-MEM containing 50 ng/ml M-CSF and 50 ng/ml RANKL for 0, 2, 4, or 6 days. The cells were fixed with 4% paraformaldehyde for 20 minutes and permeabilized with PBS containing 0.5% Triton-X for 30 minutes. For anti-BHLHE41 immunofluorescence staining, cells were blocked with PBS containing 5% BSA after fixation and permeabilization, after which the cells were incubated with primary antibody at 4°C overnight. The cells were incubated with the secondary antibody (Abcam, Cat#ab150077) for 1 hour. The images were taken with confocal microscope (Leica, SP8) and analyzed with LAS X. DAPI was used for nuclear staining.

The primary antibodies included: BHLHE41 (Affinity, Cat#AF0442, 1:200).

Transcriptomic analysis

Knock down or control group BMMs were cultured with 50 ng/ml M-CSF for 3 days, and harvested with a GenCatch TM Total RNA Extraction Kit (Epoch Life Sciences, Cat#1660050). The cDNA library was prepared and sequenced with 2μg RNA according to the manufacturer's instructions (Hiseq 2500, Illumina). HISAT2[47] was used to map sequencing reads to the mouse genome and SAMtools[48] was used to aggregate tag counts at the gene level allowing only one read per position per length. DESeq2[49] was used to determine the differentially expressed genes, the original read count was normalized, the statistical model was calculated with the hypothesis testing probability (p value), and multiple hypothesis testing was ultimately calibrated to obtain the FDR value. ClusterProfiler[50] was used to perform gene set enrichment analysis, including GO and KEGG. The enrichment analysis was based on the hypergeometric distribution principle, where the differential gene set was the differential gene set obtained from the significant difference analysis and annotated to the GO or KEGG database, and the background gene set was all the genes analyzed for significant difference and annotated to the GO or KEGG database. The results of enrichment analysis were enrichment of all differential gene sets, upregulated differential gene sets and downregulated differential gene sets for each differential comparison combination. GOplot[39] was used for the visualization of GO analysis.

Bioinformatics analysis

To explore the potential correlation between Bhlhe41 and OCs differentiation, GSE178196 (GPL18573 Illumina NextSeq 500) dataset from Gene Expression Omnibus (GEO) repository at the National Centre of Biotechnology Information website (https://www.ncbi.nlm.nih.gov/geo/) was analyzed. This data set contains three PBMCs samples treated with RANKL and M-CSF for 10d and three PBMCs samples treated with M-CSF alone. All raw expression data was standardized by R and Bioconductor (http://www.bioconductor.org) Affymetrix package. The Linear Array Microarray Analysis (Limma) software package was used to identify the differentially expressed genes (DEGs) in PBMCs samples treated with M-CSF and RANKL compared with samples stimulated with M-CSF alone. Values of $p<0.05$ and $|log2FC| >0.5$ were considered thresholds for identifying DEGs.

In order to determine the correlation of BHLHE41 and NFATc1, GSE56815 from the GEO repository at the National Center for Biotechnology Information website (https://www.ncbi.nlm.nih.gov/geo/) were used for analysis (GPL96 Affymetrix Human Genome U133A Array). GraphPad Prism 7.0 was used to analyze the correlation between BHLHE41 and NFATc1 expression.

The BHLHE41 target genes were predicted through the Gene Tranion Regulation Database (GTRD (http://gtrd.biouml.org/). The binding site of BHLHE41 was predicted through the JASPAR database.

QUANTIFICATION AND STATISTICAL ANALYSIS

Data are expressed as mean ± SD. The results were considered statistically significant if the P value was less than 0.05. The random number method was used for random assignment. Researchers were blinded to group assignment during the experiment. The cell experiments were examined in three independent replicates and the animal experiments were validated by five separate experiments. Mice in poor physical condition were excluded before grouping. The data was analyzed using the appropriate Student's t test when comparing two groups or one-way analysis of variance when comparing more than 2 groups. All statistical tests were performed using Prism 7.0 software. ns $P>= 0.05$, *$P < 0.05$, **$P < 0.01$, ***$P < 0.001$, ****$P < 0.0001$. Statistical details for each experiment are included in the figures and figure legends.